

# Self-energy analysis of frequency-dependent conductivity: Application to Pb, Nb, and MgB<sub>2</sub> in normal state

Tae-Hyoung Gimm and Han-Yong Choi\*  
*Department of Physics, BK21 Physics Research Division,  
 and Center for Nanotubes and Nanostructure Composites,  
 Sung Kyun Kwan University, Suwon 440-746, Korea.*  
 (Dated: November 20, 2018)

We propose and demonstrate a microscopic way to analyze the frequency-dependent infrared conductivity: extraction of the electron self-energy from the inversion of experimentally measured infrared conductivity through the functional minimization and numerical iterations. The self-energy contains the full information on the coherent and incoherent parts of interacting electrons and, therefore, can describe their charge dynamics even when the quasi-particle concept is not valid. From the extracted self-energy, other physical properties such as the Raman intensity spectrum and the effective interaction between electrons can also be computed. We will first demonstrate that the self-energy analysis can be successfully implemented by fitting the frequency-dependent conductivities of the simple metals such as Pb and Nb, and then calculating the effective interactions between electrons from the extracted self-energies and comparing them with those obtained from the tunneling experiments. We then present the self-energy analysis of the MgB<sub>2</sub> superconductors in normal state and clarify some of the controversies in their optical spectra. In particular, the small electron-phonon coupling constant obtained previously is attributed to an underestimate of the plasma frequency.

## INTRODUCTION

The frequency-dependent conductivity  $\sigma(\omega)$  provides one of the most valuable and detailed information on the charge dynamics in a wide class of materials. It is analyzed using either the one-component or two-component models [1]. The two-component model interprets the  $\sigma(\omega)$  as arising from a combination of two types of carriers, free and bound ones. The free carriers are modeled in terms of the Drude term and the bound ones in terms of various Lorentzian oscillators. However, the interpretation of the individual Lorentzian terms, most of which are usually due to inter-band contributions, is not straightforward.

In the one-component picture, referred to as the extended Drude model (EDM), on the other hand, the frequency dependence of the conductivity  $\sigma(\omega)$  below inter-band contributions is described by extending the phenomenological parameters of the Drude model, the effective mass  $m^*$  and scattering rate  $1/\tau$ , to be frequency dependent as [1]

$$\sigma(\omega) = \frac{ne^2}{m_b} \frac{1}{1/\tau(\omega) - i\omega m^*(\omega)/m_b}, \quad (1)$$

where  $m_b$  is the electron band mass. The EDM interprets the experimentally obtained complex conductivity  $\sigma(\omega)$  in terms of  $1/\tau(\omega)$  and  $m^*(\omega)$  determined by

$$\frac{1}{\tau(\omega)} = \frac{\omega_p^2}{4\pi} \text{Re} \left[ \frac{1}{\sigma(\omega)} \right], \quad \frac{m^*(\omega)}{m_b} = -\frac{\omega_p^2}{4\pi} \frac{1}{\omega} \text{Im} \left[ \frac{1}{\sigma(\omega)} \right], \quad (2)$$

where  $\omega_p = (4\pi ne^2/m_b)^{1/2}$  is the plasma frequency,  $n$  the electron density, and  $e$  is the electron charge. The  $\omega_p$  can be found by integrating the real part of the measured conductivity from the sum rule

$$\int_0^{\omega_{max}} d\omega \sigma_1(\omega) = \frac{1}{8} \omega_p^2, \quad (3)$$

where  $\omega_{max}$  is the cutoff frequency above which inter-band contributions begin to contribute. The subscript 1 and 2 refer to, respectively, the real and imaginary parts. The EDM has been successfully employed to analyze  $\sigma(\omega)$  of the conventional metals as well as the heavy-fermions and high- $T_c$  cuprates [2].

For a class of correlated electron systems such as the ruthenates, Sr/CaRuO<sub>3</sub>, however, the EDM breaks down and yields unphysical descriptions of the materials such as the negative effective mass [3, 4]. Similar behavior is also found for some molybdates, Sm<sub>2</sub>Mo<sub>2</sub>O<sub>7</sub> and Nd<sub>2</sub>Mo<sub>2</sub>O<sub>7</sub> [5]. These observations clearly signal the inadequacy of the EDM and call for a new way of analyzing  $\sigma(\omega)$  which can be applied to a wide class of materials. We, therefore, propose to analyze the frequency dependent infrared (IR) conductivity in terms of the electron self-energy  $\Sigma(\omega)$  instead of the phenomenological parameters of Eq. (2). The electron self-energy contains the full information on the coherent and incoherent parts of interacting electrons and, therefore, can describe the charge dynamics even when the EDM or the Fermi liquid (FL) picture is no longer valid. In this self-energy analysis (SEA) method, the electron self-energy is extracted by inverting the experimentally measured infrared conductivity through the functional minimization and numerical iterations as will be discussed in detail in Section III. The SEA may be considered as a microscopic gener-

\*To whom the correspondences should be addressed. e-mail: hychoi@skku.ac.kr

alization of the EDM, which can be applied to analyze the frequency-dependent conductivity data of the non-Fermi liquids as well as the Fermi liquids. Even for the FL where the EDM is expected to work, the SEA can yield quantitatively more reliable results than the EDM, especially for the FL with a strong electron-phonon coupling. The present paper is mainly devoted to a detailed description of the SEA method and its applications to relatively simple metals. For more complicated cases of strongly correlated electron systems including cuprates, molybdates and ruthenates, by which we were originally motivated, we plan to report the SEA results separately elsewhere. For these systems, qualitatively different results from the EDM results are expected.

After the Introduction, we will discuss the frequency-dependent conductivity  $\sigma(\omega)$  expressed in terms of the self-energy  $\Sigma(\omega)$  and its relation with the EDM in Sec. II. This will clarify the inherent limitations of the widely employed EDM analysis for the frequency-dependent conductivity. We will then describe in Sec. III the formulation of the SEA method, which is reduced to the global minimization of a  $N$ -variable function. The SEA method will be applied to experimental data of Pb, Nb and MgB<sub>2</sub> and the results are presented in comparison with the EDM analysis in Sec. IV. In Sec. V, we give a brief summary and some perspectives on the self-energy analysis method.

## OPTICAL CONDUCTIVITY AND SELF-ENERGY

The frequency-dependent conductivity  $\sigma(\omega)$  can be obtained from the current-current correlation function, and is written in terms of the electron self-energy  $\Sigma(\omega)$  as [6, 7]

$$\sigma(\omega) = \frac{\omega_p^2}{4\pi} \frac{i}{\omega} \int_{-\infty}^{\infty} d\epsilon \frac{f(\epsilon - \omega) - f(\epsilon)}{\omega - \Sigma(\omega - \epsilon) - \Sigma(\epsilon)}, \quad (4)$$

where  $f(\epsilon)$  is the Fermi distribution function. We assumed a constant density of states over an infinite bandwidth and no long-range order. It is also assumed that the momentum dependence is much weaker compared with the frequency dependence,  $\Sigma(\vec{k}, \omega) = \Sigma(\omega)$ , as in the dynamical mean-field theory, which renders the vertex correction vanish in the current-current correlation function [8].

The electron self-energy represents the effects of electron interaction with various excitations in a system. The imaginary part of the self-energy can be written as

$$\begin{aligned} \Sigma_2(\omega) = & - \int_{-\infty}^{\infty} d\Omega \left[ \coth\left(\frac{\Omega}{2T}\right) \right. \\ & \left. + \tanh\left(\frac{\omega - \Omega}{2T}\right) \right] P_2(\Omega) + \Sigma_2^{imp}, \end{aligned} \quad (5)$$

where  $\Sigma_2^{imp}$  is the frequency-independent contribution from impurities.  $P_2(\omega)$  is the imaginary part of the effective interaction satisfying  $P_2(-\omega) = -P_2(\omega)$  and  $T$  is the temperature. The isotropically weighted phonon density of states for electron-phonon coupled systems is given by

$$\alpha^2 F(\omega) = \frac{1}{\pi} P_2(\omega). \quad (6)$$

Once the self-energy is known, we use Eq. (5) to find the effective interaction spectrum  $P_2(\omega)$  using a derivative with respect to  $\omega$  at low  $T$  or a convolution after Fourier transformations [7].

In the zero temperature limit  $T = 0$ , the  $\sigma(\omega)$  of Eq. (4) is reduced to

$$\sigma(\omega) = \frac{\omega_p^2}{4\pi} \frac{i}{\omega} \int_0^\omega d\epsilon \frac{1}{\omega - \Sigma(\omega - \epsilon) - \Sigma(\epsilon)}, \quad (7)$$

which means that in the low  $T$  limit, only the self-energy  $\Sigma(\epsilon)$  between  $0 < \epsilon < \omega$  contributes to the conductivity at  $\omega$ . This may be interpreted as  $\sigma(\omega)$  being an ‘‘average’’ of  $1/[\omega - \Sigma(\epsilon) - \Sigma(\omega - \epsilon)]$  between 0 and  $\omega$ . This, in turn, suggests that the information from the EDM analysis, which is directly obtained from  $\sigma(\omega)$  using Eq. (2), is an average of the corresponding quantity from the SEA. This will be discussed in more detail below. The EDM can be obtained from Eq. (4) in an appropriate limit. The  $\sigma(\omega)$  of Eq. (4) is reduced to the EDM form of Eq. (1) with  $m^*(\omega)/m_b = 1 + \lambda(\omega)$  provided that

$$\Sigma(\omega - \epsilon) + \Sigma(\epsilon) \approx -\omega\lambda(\omega) - i/\tau(\omega) \quad (8)$$

is satisfied [9]. For a FL, where  $\Sigma_1(\omega) \approx -\lambda(\omega)\omega$  and  $\Sigma_2(\omega) \approx \Sigma_2^{imp} - \Gamma\omega^2$ , this condition can be satisfied for small  $\epsilon$  and  $\omega$ , if  $\lambda(\omega)$  has a weak  $\omega$ -dependence. Therefore, the EDM can give a satisfactory description of  $\sigma(\omega)$  for weak-coupling FL, where

$$\frac{1}{\tau(\omega)} \approx -2\Sigma_2(\omega), \quad \frac{m^*(\omega)}{m_b} \approx 1 + \lambda(\omega) \approx 1 - \frac{\partial \Sigma_1(\omega)}{\partial \omega}. \quad (9)$$

In the weak-coupling limit, where Eq. (8) is well satisfied, the optical scattering rate  $1/\tau(\omega)$  can be approximately written as [2, 9, 10]

$$\begin{aligned} \frac{1}{\tau(\omega)} \approx & \frac{2\pi}{\omega} \int_{-\infty}^{\infty} d\Omega \left[ \omega \coth\left(\frac{\Omega}{2T}\right) \right. \\ & \left. + (\omega - \Omega) \coth\left(\frac{\omega - \Omega}{2T}\right) \right] \alpha_{tr}^2 F(\Omega) + \frac{1}{\tau_{imp}} \end{aligned} \quad (10)$$

where  $1/\tau_{imp}$  is the impurity contribution and  $\alpha_{tr}^2 F(\omega)$  is a phonon density of states weighted by the amplitude for large-angle scattering on the Fermi surface, which has the same spectral structure as  $\alpha^2 F(\omega)$ , but their amplitudes can be lower. In this paper we will not distinguish the  $\alpha^2 F(\omega)$  and  $\alpha_{tr}^2 F(\omega)$  from now on. We note that there were several previous attempts to invert  $\alpha^2 F(\omega)$  [7, 11].

For instance, one may obtain  $\alpha^2 F(\omega)$  in the  $T = 0$  limit of Eq. (10) using

$$\alpha^2 F(\omega) \approx \frac{1}{2\pi} \frac{d^2}{d\omega^2} \left[ \frac{\omega}{\tau(\omega)} \right] \approx \frac{1}{2\pi} \frac{\omega_p^2}{4\pi} \frac{d^2}{d\omega^2} \text{Re} \left[ \frac{\omega}{\sigma(\omega)} \right], \quad (11)$$

where the second expression follows by using the EDM of Eq. (1). This formula, however, has limitations to be applied to the experimental IR data because large error bars are inevitable from the double differentials and it is valid only when EDM is valid and at  $T = 0$  [7].

For strong-coupling FL where  $\lambda(\omega)$  has a significant  $\omega$ -dependence, analysis based on the EDM becomes less accurate. For the marginal Fermi liquid, where  $\Sigma_1(\omega) \sim \omega \ln|\omega|$  and  $\Sigma_2(\omega) \sim -|\omega|$ , the EDM is expected to give somewhat less reliable description because  $\Sigma_1(\omega)$ , unlike FL, deviates from the linearity in  $\omega$ . The situation becomes worse for non-Fermi liquid, where  $\Sigma_1(\omega) \sim -\omega^{1-\alpha}$  and  $\Sigma_2(\omega) \sim -\omega^{1-\alpha}$  ( $0 < \alpha < 1$ ), and the EDM may give misleading and qualitatively incorrect descriptions as were observed in the ruthenates [3, 4].

## FORMULATION OF SELF-ENERGY ANALYSIS

We now present how one can analyze the frequency-dependent infrared conductivity with the formula of Eq. (4). As is explained below, the problem is reduced to a global minimization of a  $N$ -variable function. Using Eq. (4), it is simple to calculate the conductivity  $\sigma(\omega)$  from a given self-energy  $\Sigma(\omega)$ . What we are trying to do here is exactly the inverse of that: We wish to extract  $\Sigma(\omega)$  from an experimentally measured  $\sigma(\omega)$ .

The SEA is implemented by defining the functional  $W[\Sigma_2]$  as

$$W[\Sigma_2] \equiv \int_0^{\omega_c} d\omega [\sigma_1(\omega) - \sigma_1^{exp}(\omega)]^2, \quad (12)$$

where  $\sigma_1^{exp}$  and  $\sigma_1$  are the real parts of the experimental data and calculated conductivity using Eq. (4), respectively. Since the real part of self-energy  $\Sigma_1(\omega)$  can be obtained from the imaginary part  $\Sigma_2(\omega)$  by the Kramers-Kronig transformation, we can consider  $\Sigma_2(\omega)$  as the only independent function. The functional  $W$  is positive definite, and has the global minimum of zero for the self-energy which reproduces the experimental conductivity data. The self-energies defined at the  $N$  discrete frequencies,  $x_i \equiv \Sigma_2(\omega_i)$  for  $i = 1, \dots, N$  ( $\omega_N = \omega_c$ ), are taken as the  $N$  independent variables of the function  $W(x_1, x_2, \dots, x_N) \equiv W[\Sigma_2]$ . The cutoff frequency  $\omega_c$  is not necessarily equal to the  $\omega_{max}$  of Eq. (3). Now, the problem is reduced to a global minimization of a  $N$ -variable function.

We note that, depending on the problems, other forms of the functional  $W$  may yield better results. For good

metals, for instance, whose mid-IR conductivity is very small compared with far-IR region,

$$W = \int_0^{\omega_c} d\omega [\ln \sigma_1(\omega) - \ln \sigma_1^{exp}(\omega)]^2 \quad (13)$$

works better than the form of Eq. (12). For the region where  $\omega > \omega_c$ , which we need to know for the Kramers-Kronig transformation,  $\Sigma_2(\omega)$  is taken as constant. A constant  $\Sigma_2(\omega)$  for  $\omega > \omega_c$  corresponds to the reflectivity  $R(\omega) \sim 1/\omega^4$ , which is consistent with the standard procedure in the IR experiments.

The global minimization of  $W$  is achieved via the functional derivative and numerical iterations. We start with an initial configuration of  $x_i^{(0)}$ . A good initial guess can be  $x_i^{(0)} = -\frac{1}{2\tau(\omega_i)}$  obtained from EDM analysis, or a negative constant value for the whole frequency range. Then, we move to new  $x_i$  along the steepest descent direction of  $W$ .

$$x_i^{(new)} = x_i^{(old)} - s \left. \frac{dW}{dx_i} \right|_{x_i=x_i^{(old)}}, \quad (14)$$

where  $\frac{dW}{dx_i}$  represents the functional derivative of the functional  $W[\Sigma_2]$  with respect to  $\Sigma_2(\omega)$  given by

$$\begin{aligned} \frac{dW}{dx_i} &= 2 \int_0^{\omega_c} d\omega' [\sigma_1(\omega') - \sigma_1^{exp}(\omega')] \Delta|_{\omega=\omega_i}, \\ \Delta &\equiv \frac{\delta \sigma_1(\omega')}{\delta \Sigma_2(\omega)} + \frac{1}{\pi} \int_{-\infty}^{\infty} d\epsilon \frac{\delta \sigma_1(\omega')}{\delta \Sigma_1(\epsilon)} \mathcal{P} \frac{1}{\omega - \epsilon}, \end{aligned} \quad (15)$$

where  $\mathcal{P}$  stands for the principal value, and the use is made of  $\frac{\delta \Sigma_1(\epsilon)}{\delta \Sigma_2(\omega)} = \frac{1}{\pi} \mathcal{P} \frac{1}{\omega - \epsilon}$ . The step size  $s$  is chosen such that the  $W$  is maximally decreased along the steepest descent direction. The  $\omega_p^2$ , which sets the scale of  $\sigma(\omega)$  of Eq. (4) is updated at each iteration such that the calculated spectral sum is equal to the experimental spectral sum up to  $\omega_c$ . Note that this way of determining  $\omega_p$  does not require that  $\omega_c = \omega_{max}$  of Eq. (3) and, therefore, the extracted  $\omega_p$  is almost independent of  $\omega_{max}$  and more reliable than that from the sum rule of Eq. (3). This enables us to determine  $\omega_p$  more systematically as we will discuss in more detail below.

In general, the global minimization of a few hundred independent variables is an extremely demanding problem. In the present case, however, it is rendered tractable because of the following observations: (1) We know the value of the global minimum unlike general global minimization problems. It is exactly zero. (2) We have some ideas about the physically meaningful form of the  $\Sigma_2(\omega)$ . It should be a continuous function of the frequency and negative definite. (3) We have a better way to escape from local minima than trying a new random starting point,  $x_i^{(0)}$ : Take  $\Sigma_2^{(new)}(\omega) - \Sigma_2^{(old)}(\omega) \propto \sigma_1(\omega) - \sigma_1^{exp}(\omega)$ . An estimation of this process can be obtained in following way. The contribution to the conductivity at a given frequency  $\omega$  is dominated by the self-energy below  $\omega$  in

the low temperature limit due to the thermal factor of  $[f(\epsilon - \omega) - f(\epsilon)]/\omega$  of Eq. (4) as discussed in Eq. (7). By modifying the self-energy to be proportional to the difference between calculated conductivity and the experimental data at each frequency, we can continue our minimization modifying the ‘wrong’ region without spoiling a ‘good’ region.

From the extracted  $\Sigma(\omega)$ , other physical properties such as the plasma frequency, effective interaction between electrons, Raman spectra, and inelastic neutron scattering intensity can also be calculated. For instance, we use Eq. (5) to find the effective interaction spectrum  $P_2(\omega)$  from an extracted  $\Sigma_2(\omega)$  which was discussed in the previous section. An important byproduct of the SEA is that the plasma frequency  $\omega_p$  can be determined more accurately than has been *hitherto* practiced, which is necessary to determine the Drude parameters of Eq. (2). Conventionally,  $\omega_p$  is determined by  $\omega_{max}$  of Eq. (3) which, in turn, is taken such that the sum as a function of  $\omega_{max}$  has the smallest slope. This procedure can be problematic especially for the materials without a sharp plasma edge in the reflectivity data. In contrast, SEA works in this case as well because the determination of  $\omega_p$ , which sets the scale of  $\sigma(\omega)$ , is almost *independent* of the  $\omega_c$  of the functional  $W$ . For instance, one can determine  $\omega_p$  with only very restricted data between  $0 < \omega < \omega_c$  ( $\ll \omega_{max}$ ). This will be illustrated for Nb below.

Another byproduct closely related to the  $\omega_p$  determination is that we may separate the intra- and inter-band contributions more systematically. We can extract the self-energy of effective single-component carriers by fitting the low-frequency experimental conductivity up to  $\omega_c \approx \omega_{max}$ . The conductivity  $\sigma(\omega)$  calculated by substituting the extracted  $\Sigma(\omega)$  into Eq. (4) is intra-band conductivity. This process, however, is more sensitive to  $\omega_c$  than the  $\omega_p$  determination.

We will demonstrate in the next section that the SEA is straightforward to implement to extract the self-energy from experimental IR conductivity without the local minimum problem. We have found that the SEA yields the same solution  $\Sigma_2(\omega)$  from almost any initial configuration. The obtained solution  $\Sigma_2(\omega)$ , therefore, seems unique.

## APPLICATIONS TO EXPERIMENTAL DATA

We will now apply the SEA developed in the previous section to real materials, and demonstrate that it can be readily employed to analyze the frequency-dependent IR experimental data. In the first two parts of this section, we will analyze the simple metals, Pb and Nb. From the SEA, we can extract the self-energy of the materials, and from the extracted self-energy we can find the  $\alpha^2 F(\omega)$  using Eqs. (5) and (6). It can be compared with

the measured  $\alpha^2 F(\omega)$  well established from the tunneling experiments [12]. But for such a good metal, it is a very demanding task to measure the conductivity in far-IR region, since the reflectivity is very close to 100 % there. Thus there exist few published conductivity data for Pb and Nb. For Pb, we take the experimental  $\alpha^2 F(\omega)$  obtained from the tunneling experiment and calculate the self-energy from Eqs. (5) and (6), and then calculate the conductivity from Eq. (4). This is taken as the “experimental” conductivity  $\sigma^{exp}(\omega)$  for Pb. After that, the real experimental data of Nb is analyzed [13]. The results are compared with those obtained from the tunneling spectra. The last part of this section is devoted to the SEA for the normal state IR conductivity data of MgB<sub>2</sub> superconductor. We will argue from the SEA results that the small electron-phonon coupling constant  $\lambda$  extracted previously from the  $T$ -dependence of the resistivity  $\rho(T)$  and EDM analysis of  $\sigma(\omega)$ , which is too small to account for the superconducting transition temperature  $T_c$ , is most likely due to an underestimate of the plasma frequency  $\omega_p$ .

### Application to Pb: Generated data

We take Pb as a test case of the proposed SEA because its  $\alpha^2 F(\omega)$  is well established from the tunneling [12]. The electron-phonon coupling constant  $\lambda$  of this metal is known to be  $\approx 1.5$ . The frequency-dependent IR conductivity of Pb, however, is not available. Therefore, the IR conductivity data was generated with Eqs. (4) and (5) using the tunneling  $\alpha^2 F(\omega)$  at 200 frequencies up to  $\omega_c = 15$  meV with an equal spacing. We took the self-energy due to impurity scattering  $\Sigma_2^{imp} = -1$  meV and  $T = 3$  K as representative values. The generated conductivity in this way, shown in the left column of Fig. 1 with open circle, is taken as the “experimental” data  $\sigma_1^{exp}(\omega)$ . It was then fitted by the SEA as explained above to extract the self-energy  $\Sigma_2(\omega_i)$  without, of course, any information about the self-energy used to generate the conductivity. The results are shown in the solid line in the left column of Fig. 1. The extracted and experimental conductivities are almost indistinguishable. Note that the width (HWHM) of  $\sigma_1(\omega)$  is not given by  $-2\Sigma_2(\omega = 0)$  because of the substantial frequency dependence of  $\Sigma_2(\omega)$ .

In the right column of Fig. 1, we show the real and imaginary parts of the extracted self-energy in the forms of  $-2\Sigma_2(\omega)$  and  $1 - \Sigma_1(\omega)/\omega$ , along with the generated experimental data. The extracted and experimental data are shown, respectively, by the solid line and open circles. They are practically indistinguishable. For comparison, we also plotted the EDM analysis of the experimental conductivity data,  $1/\tau(\omega)$  and  $m^*(\omega)/m_b$ , in dotted lines, using Eq. (2). As discussed in Eq. (9),  $1/\tau(\omega)$  and  $m^*(\omega)/m_b$  correspond, respectively,  $-2\Sigma_2(\omega)$

and  $1 - \Sigma_1(\omega)/\omega$ . The right panel demonstrate, however, that they can substantially deviate from each other even for the relatively simple metals. The EDM analysis in general yield smoother frequency dependences for  $1/\tau(\omega)$  and  $m^*(\omega)/m_b$ . This is expected because  $1/\tau(\omega)$  is an “average” of the  $\Sigma_2(\omega)$  as discussed previously in Section II. The curve shown by the thin solid line in the lower picture was calculated by using the approximate formula Eq. (10), which is in a good agreement with the  $1/\tau(\omega)$  from the EDM analysis [9].

From the extracted self-energy,  $\alpha^2 F(\omega)$  can be obtained from a derivative with respect to  $\omega$ ,  $\alpha^2 F(\omega) = -\frac{1}{\pi} \frac{\partial \Sigma_2(\omega)}{\partial \omega}$ , which is valid at low  $T$  (dotted curve) or a convolution of Eq. (5) (thin solid curve) [7] as shown in the upper left inset of Fig. 1. The experimental  $\alpha^2 F(\omega)$  is shown in the thick solid line. The extracted  $\alpha^2 F(\omega)$  from the convolution is again almost indistinguishable from the experimental one. These results from the SEA show substantial improvements over the previous attempts [11] based on the assumptions of both  $T = 0$  and weak-coupling limit. We argue from this example that even for the simple metals, for which the EDM can give the qualitatively valid description, the SEA can provide more accurate and reliable description of the material, which can be quite different from the EDM results.

### Application to Nb

We now proceed to apply the present method to the experimental IR data of Nb. We used the far-IR conductivity data measured by Pronin *et al.* in the normal state at 9 K [13]. Their far-IR data are available from 84 up to 300  $\text{cm}^{-1}$  (with constant data in the DC limit measured via a different method), which is a good example to demonstrate that the  $\omega_p$  can be obtained without a full intra-band spectrum in the SEA.

We took  $\omega_c = 250 \text{ cm}^{-1}$  and  $N = 200$ . For  $0 \leq \omega \leq 84 \text{ meV}$ , we constrain  $\Sigma_2(\omega)$  to remain constant. This implies vanishing  $\alpha^2 F(\omega)$  in the region as shown in the upper right inset of Fig. 2 and, consequently, a reduced  $\lambda$ , and the Drude behavior in  $\sigma_1(\omega)$ . The fitted (solid curve) and experimental (crosses)  $\sigma_1(\omega)$  are plotted in Fig. 2. The electron-phonon coupling constant  $\lambda = -\partial \Sigma_1(\omega)/\partial \omega|_{\omega \rightarrow 0}$  from the SEA is 0.51 which is somewhat reduced compared with the experimental value of  $0.9 - 1$  [12] as discussed above. The calculated plasma frequency is 7.8 eV while the experimental value is 7.2 eV [13]. In the lower left inset, the extracted  $\Sigma_2(\omega)$  is shown. The above results clearly demonstrate that the SEA works also for the case with only restricted data.

These two examples of the SEA establish that the method can indeed be applied to analyze the frequency conductivity and it can provide the most microscopic information of interacting electron systems, the self-energy  $\Sigma(\omega)$  and the effective interaction  $P(\omega)$ . The SEA can

provide for the Fermi liquids more reliable and accurate information than the conventional EDM analysis. For the non-Fermi liquids, it is expected to provide qualitatively different information which is *not* accessible with the EDM.

### Application to $\text{MgB}_2$

Let us now analyze the IR data of normal state  $c$ -axis oriented  $\text{MgB}_2$  film measured by Tu *et al.* [14], which we regard as being due to intra-band excitations of an effective single band system [7]. In Fig. 3(a), the experimental conductivities of Tu *et al.* at  $T = 45 \text{ K}$  and  $295 \text{ K}$  are shown together with the fitted conductivities using the SEA with  $N = 300$  and  $\omega_c = 6000 \text{ cm}^{-1}$ . The solid curves represent the fitted conductivities, and the dashed and dotted curves, respectively, the experimental ones at  $T = 295 \text{ K}$  and  $T = 45 \text{ K}$ . The small discrepancies are due to phonons. In Fig. 3(b), the results from the EDM analysis are shown in the left column, and those from the present SEA in the right column. The solid and dashed curves are, respectively, for  $T = 45 \text{ K}$  and  $295 \text{ K}$ . Tu *et al.* found from the sum rule of Eq. (3) that  $\omega_p$  is  $14750 \text{ cm}^{-1}$  which yields, through the EDM, a very weak electron-phonon coupling as shown in the left column of Fig. 3(b). They obtained  $\lambda_{tr} \approx 0.13$  using the Bloch-Grüneisen formula to analyze the  $T$ -dependence of the resistivity, which is consistent with the EDM analysis [14, 15]. To the extent that  $\lambda_{tr} \approx \lambda$ , it seems too small to account for the superconducting transition temperature  $T_c = 39 \text{ K}$ . On the other hand, we found from the SEA that  $\lambda \approx 0.56$  and  $0.41$  at, respectively,  $T = 45$  and  $295 \text{ K}$  as shown in Fig. 3(b), which are substantially larger than what Tu *et al.* found. The local density approximation calculation yields  $\lambda_{tr} \approx 0.6$  [16]. One way of seeing the discrepancy between EDM and SEA is that the  $\omega_p$  from SEA is larger than that from EDM. We found that  $\omega_p = 16690 \text{ cm}^{-1}$  at  $T = 45 \text{ K}$ , and  $16740 \text{ cm}^{-1}$  at  $T = 295 \text{ K}$ . If the enhanced  $\omega_p$  are used in the EDM, the resulting  $\lambda_{tr}$  are in good agreement with the SEA. As far as the EDM and the  $T$ -dependence of the resistivity are concerned, the enhanced  $\omega_p$  resolves the problem of the small  $\lambda_{tr}$ .

With the SEA, we may go further and perform the spectral analysis to see the frequency range that contributes to  $\lambda$ , which can *not* be carried out with the EDM analysis.  $\lambda = 2 \int_0^\infty d\Omega \frac{\alpha^2 F(\Omega)}{\Omega}$ , where  $\alpha^2 F(\omega) = \frac{1}{\pi} P_2(\omega)$  may be obtained from the extracted  $\Sigma_2(\omega)$  using Eq. (5). The  $-2\Sigma_2(\omega)$  is shown in the right column of Fig. 3(b). The extracted  $\alpha^2 F(\omega)$  is shown in Fig. 4 together with those from tunneling [17] (dashed line) and LDA calculation [16] (thin solid line). They are shown in a wider frequency range in the inset. The extracted  $\alpha^2 F(\omega)$  from SEA are characterized by two frequency regions which make dominant contributions to  $\lambda$ ; around  $\omega \approx$

70 and 300 meV, which is, interestingly, consistent with the model proposed by Marsiglio [15]. The low frequency region around 70 meV is the contribution from the  $E_{2g}$  phonon mode, while the nature of the high frequency region is not clear. The two regions contribute almost equally to  $\lambda$ :  $\lambda_{\text{phonon}} \approx 0.36$  (0.21) and the total  $\lambda$  is 0.56 (0.41) for  $T = 45$  K ( $T = 295$  K).

The extracted  $\alpha^2 F(\omega)$ , compared with the local density approximation (LDA) calculation, correctly captured the main  $E_{2g}$  contribution but missed smaller contributions from other phonon modes; among the modes in the  $\alpha^2 F(\omega)$  obtained from the LDA calculation shown in Fig. 4, the modes whose  $\alpha^2 F(\omega)$  are smaller than  $\sim 0.5$  are absent in the SEA results. This, we suspect, may be a consequence of the broad features around 160 and 880  $\text{cm}^{-1}$  in the experimental  $\sigma(\omega)$ , which were *not* predicted by phonon calculations [14] and possibly due to MgO impurities. We did not eliminate these contributions for the present calculations. This may smear out otherwise sharper frequency dependence of  $\sigma(\omega)$ , and reduce the electron-phonon coupling constant.

Apart from these discrepancies, the SEA successively describes the frequency-dependent conductivity of the  $\text{MgB}_2$  and yields an increased  $\lambda$  than the previous estimate. The SEA suggests, which made more accurate determination of  $\omega_p$  possible, that the small  $\lambda$  reported in the  $c$ -axis oriented sample is most likely due to underestimated  $\omega_p$ , and the total  $\lambda$  from the SEA is substantially larger. However, the  $\lambda_{\text{phonon}} \approx \lambda/2$  still seems a bit too small to account for the  $T_c$ .

## SUMMARY AND DISCUSSIONS

In this paper we have proposed and demonstrated a microscopic way to analyze the frequency-dependent infrared conductivity, referred to as self-energy analysis, which is valid for the non-Fermi liquids as well as the Fermi liquids. Additional advantage of the self-energy analysis is that the plasma frequency  $\omega_p$  can be obtained with a better accuracy. Through the self-energy analysis, we extracted the electron self-energy from the inversion of experimentally measured infrared conductivity, and the effective interaction between electrons from the extracted self-energy. After we demonstrated that the self-energy analysis method can be successfully applied for simple metals like Pb and Nb, we applied the method to the IR conductivity data of normal state  $\text{MgB}_2$ . We have found that the  $\lambda$  from the self-energy analysis is substantially larger than that obtained from the conventional analysis of the  $T$ -dependence of the resistivity and extended Drude model. The discrepancies between the self-energy analysis and conventional method for  $\text{MgB}_2$  is attributed to the underestimated  $\omega_p$  from the conventional method. However, the  $\lambda_{\text{phonon}}$  from the self-energy analysis still seems a bit small to account for the  $T_c$ .

Now that we have demonstrated that the self-energy analysis of the frequency-dependent infrared conductivity really works and can be very powerful, some concluding remarks and outlooks are in order. First, one may wonder if the solution to the global minimization of the functional  $W[\Sigma_2]$  is unique. The answer seems positive: the converged solutions, with different initial configurations, of given conductivity data all agree with each other. This means that the extracted self-energy  $\Sigma_2(\omega)$  is indeed unique. Second, we have also checked if there is any spurious feature from the Kramers-Kronig transformation used in the present work to obtain the real part of the self-energy from the imaginary part. We therefore have fitted the complex conductivity by treating both the real and imaginary parts of  $\Sigma(\omega)$  as independent variables, which eliminates the use of Kramers-Kronig. This gives the same  $\Sigma_2(\omega)$  with the procedure using  $W[\Sigma_2]$ , demonstrating the reliability of the present method. Third, we plan to report results of the self-energy analysis of the conductivity for other correlated electron systems such as the high  $T_c$  superconductors,  $\text{Sm}_2/\text{Nd}_2\text{Mo}_2\text{O}_7$ , and  $\text{Ca}/\text{SrRuO}_3$  mentioned in the introduction. The differences between the self-energy analysis and the extended Drude model analysis are expected to be *quantitative* for the Fermi liquids, but be *qualitative* for the non-Fermi liquids. It will therefore be very interesting to see what information the self-energy analysis provide for the strongly correlated electron systems. Also among the plan are extending the self-energy analysis to non constant density of states and broken symmetry states, and doing the analysis for other two-particle probes such as the electronic Raman and inelastic neutron spectra. We believe that the self-energy analysis seems timely and urgent in view of the mounting interests in the correlated electron or non-Fermi liquid systems for which the phenomenological analyses may yield inadequate results.

We would like to thank J. J. Tu and A. V. Pronin for providing their experimental data for our analyses. We also thank Tae Won Noh, Jae-Hoon Kim, In-Sang Yang, Jaejun Yu, Yunsang Lee, Mi-Ock Mun, Jooyoung Lee, Seki Kim, M. J. Rice, D. van der Marel, D. B. Tanner, T. Timusk, F. Marsiglio, S. V. Shulga, and S. L. Cooper for helpful comments and discussions. This work was supported by the Korea Science & Engineering Foundation (KOSEF) through grant No. R01-1999-000-00031-0 and CNNC, and by the Ministry of Education through BK21 SNU-SKKU program.

- 
- [1] D. B. Tanner and T. Timusk, in *Physical Properties of High Temperature Superconductors* Vol. III (World Scientific, 1992), p. 363.
  - [2] A. V. Puchkov, D. N. Basov, T. Timusk, J. Phys. Cond. Matt. **8**, 10049 (1996).

- [3] P. Kostic, Y. Okada, N. C. Collins, Z. Schlesinger, J. W. Reiner, L. Klein, A. Kapitulnik, T. H. Geballe, and M. R. Beasley, Phys. Rev. Lett. **81**, 2498 (1998).
- [4] Y.-S. Lee, J. Yu, J. S. Lee, T. W. Noh, T.-H. Gimm, and H.-Y. Choi, Phys. Rev. B. **66**, 41104 (2002).
- [5] M.-W. Kim and T. W. Noh, preprint.
- [6] S. B. Nam, Phys. Rev. **156**, 470 (1967); *ibid*, 487 (1967).
- [7] S. V. Shulga, cond-mat/0101243; *High- $T_c$  Superconductors and Related Materials*, ed. by S. L. Drechsler and T. Mishonov, pp. 323-360 (Kluwer Academic Publishers, Dordrecht, 2001).
- [8] A. Georges, G. Kotliar, W. Krauth, M. J. Rozenberg, Rev. Mod. Phys. **68**, 13 (1996).
- [9] S. V. Shulga, O. V. Dolgov, and E. G. Maksimov, Physica C **178**, 266 (1991).
- [10] P. B. Allen, Phys. Rev. B **3**, 305 (1971).
- [11] F. Marsiglio, T. Startseva, J. P. Carbotte, Phys. Lett. A **245**, 172 (1998); F. Marsiglio, J. Supercond. **12**, 163 (1999).
- [12] E. L. Wolf, *Principles of Electron Tunneling Spectroscopy* (Oxford University Press, N.Y., 1996).
- [13] A. V. Pronin, M. Dressel, A. Pimenov, A. Loidl, I. V. Roshchin, and L. H. Greene, Phys. Rev. B **57**, 14416 (1998).
- [14] J. J. Tu, G. L. Carr, V. Perebeinos, C. C. Homes, M. Strongin, P. B. Allen, W. N. Kang, E.-M. Choi, H.-J. Kim, and S.-I. Lee, Phys. Rev. Lett. **87**, 277001 (2001).
- [15] F. Marsiglio, Phys. Rev. Lett. **87**, 247001 (2001).
- [16] A. Y. Liu, I. I. Mazin, J. Kortus, Phys. Rev. Lett. **87**, 087005 (2001).
- [17] A. I. D'yachenko, V. Y. Tarenkov, A. V. Abal'oshev, S. J. Lewandowski, cond-mat/0201200.

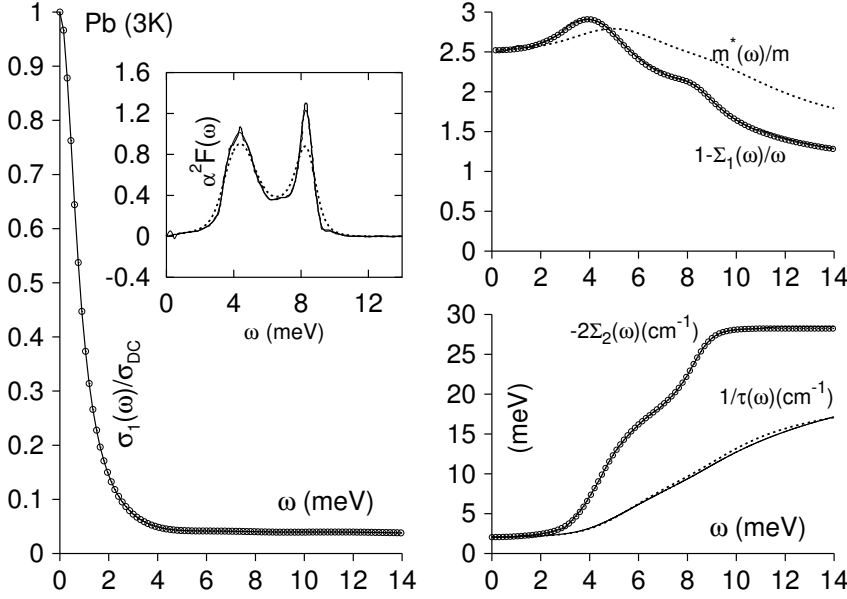


FIG. 1: Left:  $\sigma_1(\omega)$  is plotted for Pb with  $\Sigma_2^{imp} = -1$  meV and at  $T = 3$  K. The extracted and generated conductivities are shown, respectively, in solid line and open circles. The dashed and thin solid curves in the inset were obtained from, respectively,  $\alpha^2 F(\omega) = -\frac{1}{\pi} \frac{\partial \Sigma_2(\omega)}{\partial \omega}$  and the convolution using Eq. (5), and the latter is almost indistinguishable with the input tunneling data (solid line). Right: The  $1 - \Sigma_1(\omega)/\omega$  and  $-2\Sigma_2(\omega)$  obtained from the SEA are plotted, respectively, in the upper and lower panels. The extracted (generated) ones are shown in solid line (open circles). These SEA analysis results are compared with the EDM results. The dotted lines represents  $1/\tau(\omega)$  and  $m^*(\omega)/m_b$ , respectively, obtained from EDM using the generated conductivity.  $1/\tau(\omega)$  (thin solid line) calculated by using Eq. (10) is also shown in the lower right panel for comparison.



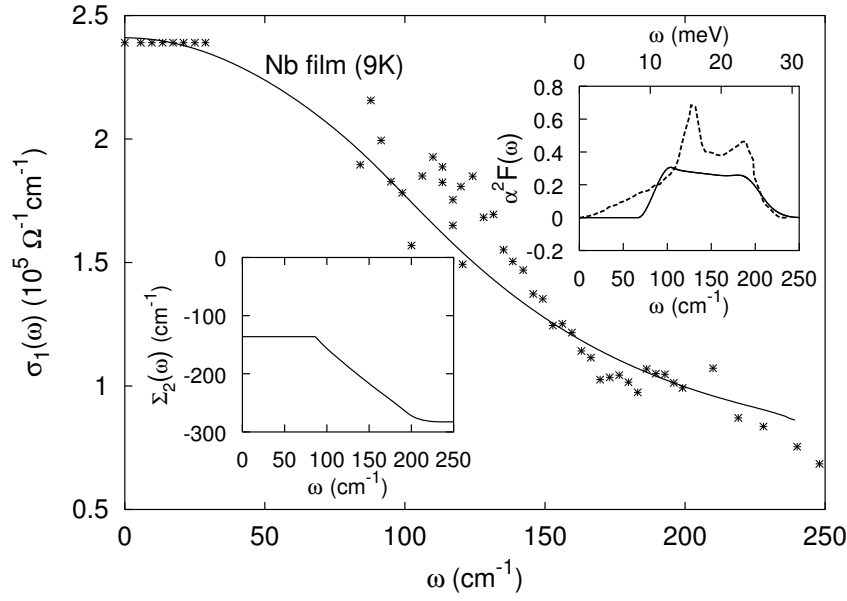


FIG. 2: The calculated and experimental  $\sigma_1(\omega)$  of Nb are shown with solid curve and crosses, respectively. In the insets, the extracted  $\alpha^2 F(\omega)$  and  $\Sigma_2(\omega)$  are shown along with the tunneling  $\alpha^2 F(\omega)$  (dashed).

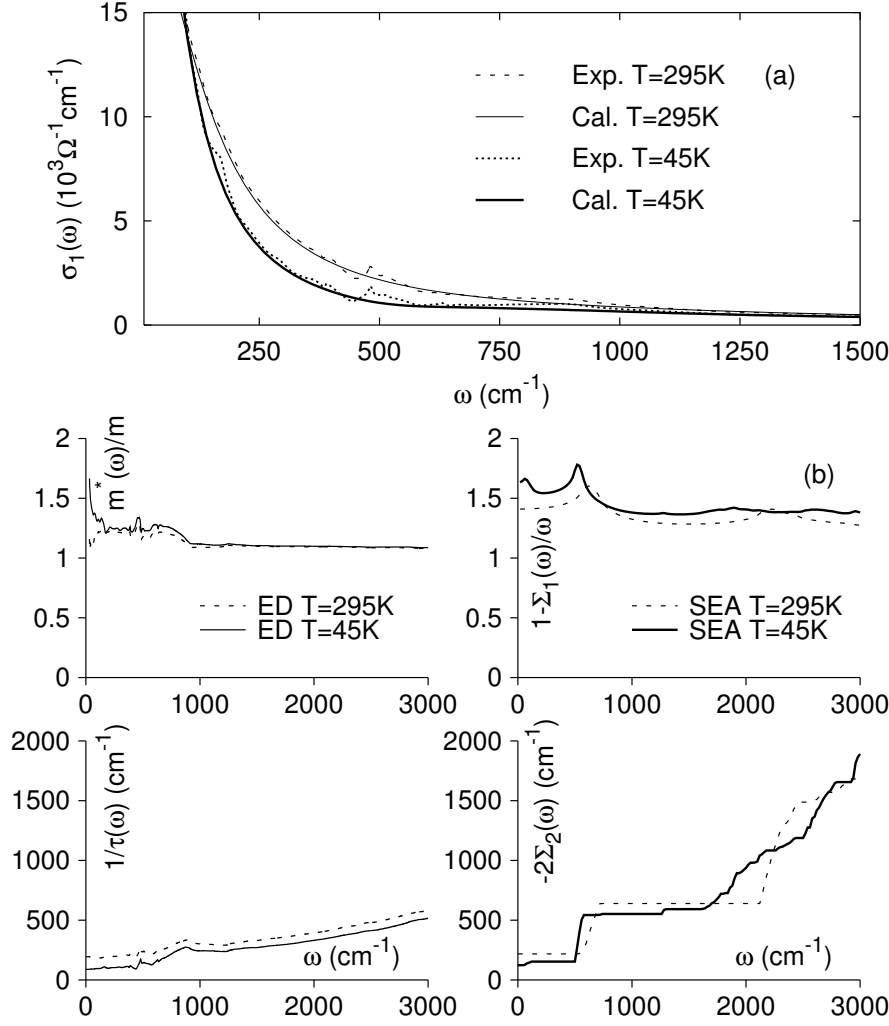


FIG. 3: (a) The calculated and measured  $\sigma_1(\omega)$  of  $\text{MgB}_2$  for  $T = 45$  and  $295 \text{ K}$ . The small discrepancies are due to phonons. (b) Left: extended Drude analysis of experimental data indicating the weak electron-phonon coupling. Right: the corresponding quantities from the self-energy analysis. Note that  $m^*/m_b$  and  $1/\tau(\omega)$  show much smoother frequency dependence compared with the corresponding  $1 - \Sigma_1(\omega)$  and  $-2\Sigma_2(\omega)$  as noted previously for Pb in Fig. 1.

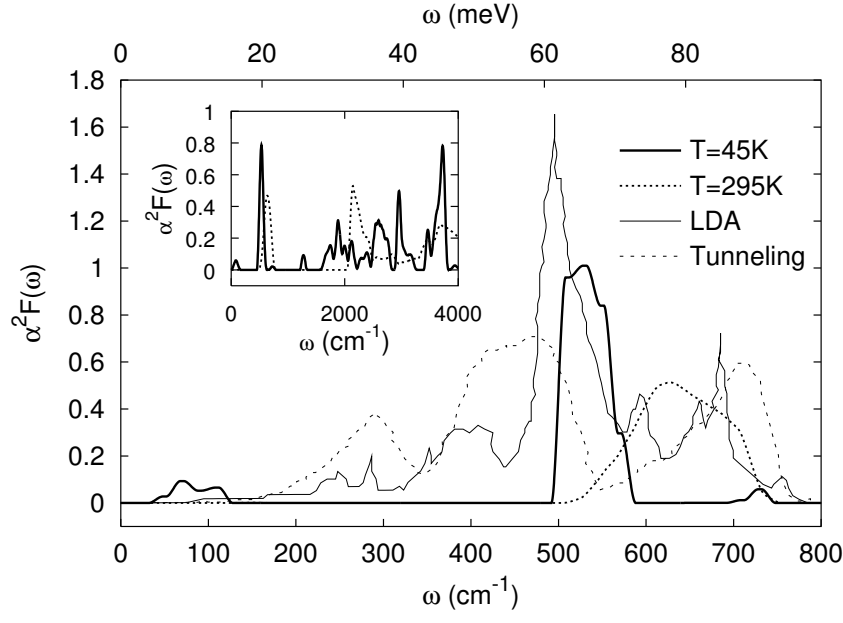


FIG. 4: The extracted  $\alpha^2 F(\omega)$  from  $\Sigma_2(\omega)$  of Fig. 3 along with those from LDA and tunneling. The extracted  $\alpha^2 F(\omega)$  shown in a wider frequency range in the inset are characterized by two dominant contributions around  $\omega \approx 70$  and  $300$  meV.